Journal of the European Ceramic Society 40 (2020) 5339–5348

Contents lists available at ScienceDirect

Journal of the European Ceramic Society

journal homepage: www.elsevier.com/locate/jeurceramsoc

Original Article

Novel nanoceramics from *in situ* made nanocrystalline powders of pure nitrides and their composites in the system aluminum nitride AlN/gallium nitride GaN/aluminum gallium nitride $Al_{0.5}Ga_{0.5}N$

Mariusz Drygas[a], Katarzyna Kapusta[a], Jerzy F. Janik[a,*], Miroslaw M. Bucko[b], Stanislaw Gierlotka[c], Svitlana Stelmakh[c], Bogdan Palosz[c], Zbigniew Olejniczak[d]

[a] AGH University of Science and Technology, Faculty of Energy and Fuels, al. Mickiewicza 30, 30-059 Krakow, Poland
[b] AGH University of Science and Technology, Faculty of Materials Science and Ceramics, al. Mickiewicza 30, 30-059 Krakow, Poland
[c] Institute of High Pressure Physics, Polish Academy of Sciences, ul. Sokolowska 29/37, 01-142 Warszawa, Poland
[d] Institute of Nuclear Physics, Polish Academy of Sciences, ul. Radzikowskiego 152, 31-342, Krakow, Poland

ARTICLE INFO

Keywords:
Nitrides
Composites
Sintering
Nanoceramics
Vicker's hardness

ABSTRACT

Presented are investigations of *in situ* preparation of composite nanopowders of AlN, GaN, and, optionally, solid solution $Al_{0.5}Ga_{0.5}N$, which were used in no-additive, high-pressure/high-temperature sintering. Two precursor synthesis pathways and two nitridation temperatures afforded nanopowders containing both (i) mixed AlN and GaN and (ii) such AlN and GaN admixed with $Al_{0.5}Ga_{0.5}N$ as well as (iii) reference individual AlN and GaN. The applied sintering temperatures were either to preserve powder nanocrystallinity (650 °C) or promote crystallite growth and sintering-mediated $Al_{0.5}Ga_{0.5}N$ formation (1000 °C). One specific route led to the novel nanoceramics of $Al_{0.5}Ga_{0.5}N$. The powders and nanoceramics were characterized by XRD, FT-IR, SEM/EDX, $^{27}Al/^{71}Ga$ MAS NMR, BET/BJH surface areas, and helium densities. Vicker's hardness tests confirmed many of the sintered composites and individual nitrides having high hardness comparable with monocrystalline AlN and GaN. Formation of pure $Al_{0.5}Ga_{0.5}N$ nanoceramics was associated with closed pore evolution and had a detrimental effect on hardness.

1. Introduction

Man-made nitrides constitute a group of fascinating materials of essential application potentials [1]. Many of them are semiconductors of which properties often surpass those of the XX century semiconductor – silicon Si. The examples include the wide bandgap semiconductor gallium nitride GaN, E_g = 3.4 eV, playing the crucial role in the modern Blu-Ray technology and energy saving LEDs, the latter being closer and closer to efficient and affordable white light sources in common-day practice [2]. Under ambient conditions, GaN can crystalize in the stable hexagonal, wurzite-type 2H form and in the metastable regular, sfalerite-type 3C form or as a mixture of the two polytypes [3]. For extremely small crystallite sizes of the order of a few nanometers, it can also be formed as defected phase inhomogeneous structures, somewhat between the hexagonal and regular varieties [3b]. On the other side, aluminum nitride AlN is, practically, an electrical insulator mainly synthesized as the hexagonal, wurzite-type variety while there have been some indications of cubic polytype formation as well [4]. Its remarkable property is the high thermal conductivity over twice that of silicon, which is outstanding among insulators. Similar to diamond, it shows negative electron affinity, advantageous thermal stability, and mechanical toughness. Given all this, it is tempting to make and explore these two nitrides composites that dwell on unique sets of properties all-in-one, for instance, a combination of semiconducting (GaN) and insulating properties with high thermal conductivity (AlN).

The binary system AlN-GaN is known under certain conditions to form solid solutions $Al_xGa_{1-x}N$, $0 < x < 1$, in the entire composition range, which may introduce such a nitride component in the-then ternary system [5]. In this regard, our previous contribution pertaining a specific precursor chemistry to AlN, GaN, and $Al_xGa_{1-x}N$ confirmed that in the mixed solutions of the dimeric Al- and Ga-tris(dimethylamides), $\{M[N(CH_3)_2]_3\}_2$, M = Al, Ga, Al:Ga = 1:1, rather slow formation of a bimetallic/mixed Al/Ga-tris(dimethylamide) dimer took place, *i.e.*, from no detectable quantities after tents of minutes to hours past mixing at room temperature (conservative equilibration conditions) to

* Corresponding author.
E-mail address: janikj@agh.edu.pl (J.F. Janik).

https://doi.org/10.1016/j.jeurceramsoc.2020.06.015
Received 27 April 2020; Accepted 5 June 2020
Available online 08 June 2020

some 50 % after a several hour reflux in pentane/hexane solutions (forced equilibration conditions) [6b]. Upon solvent removal, these dimethylamides were reacted with liquid ammonia (transamination) to afford at room temperature the metals amides-imides mixed on the molecular level either as individual species or with some proportion of the bimetallic moieties. In the subsequent deamination steps, including nitridation pyrolysis, the amides-imides and imides were eventually converted to the nanocrystalline nitrides with no separation efforts. The transamination of the metal dimethylamides (for simplicity shown as monomers) and deamination/nitridation steps constitute a sequence of the related reactions as seen below.

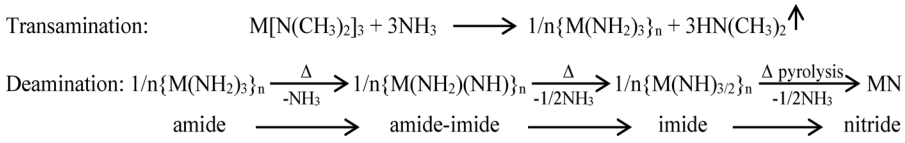

In this regard, in the case of the bimetallic Al/Ga-tris(dimethylamide), it is likely that the resulting polymeric imides may also contain the bimetallic {-(NH)-Ga-(NH)-Al-(NH)-}$_n$ linkages that will further undergo deanimation reactions at increased temperatures (nitridation) and structurally favor a formation of the nitrides' solid solution $Al_xGa_{1-x}N$. On the other hand, for the intimately mixed individual imides of {-(NH)-Ga-(NH)-}$_n$ and {-(NH)-Al-(NH)-}$_n$, a prevailing formation of separate nanosized AlN and GaN in the composite mixture is expected although suitably high nitridation temperatures may push the reactions of the nitrides towards some solid solution formation, too. In conclusion of this aspect, the binary nitride system AlN-GaN may become more complex by way of a partial or even complete solid solution $Al_xGa_{1-x}N$ formation in the nitrides preparation stage. It is worth to note that, here, the intimately homogenized binary or ternary nitride nanocomposites are made *in situ* in one processing sequence of the molecularly mixed individual or bimetallic dimethylamide precursors.

Powder sintering constitutes a viable way to make mechanically compact and machinable materials which, for example, could serve in certain applications as economical substitutes for difficult to make and expensive monocrystals or vapor phase deposited thin films. It is not only a matter of conventional ceramics made from microcrystalline powders but it extends now to new nanoceramics prepared from nanopowders [7]. In general, metal/metalloid nitride powder sintering is a challenging task and it has been usually accomplished by using suitable sintering additives such as low melting oxides forming eutectic liquid phases that act as particle binding agents. This is especially true for, arguably, the most extensively elaborated to-date sintering of silicon nitride Si_3N_4 with additives of various metal oxides and, sometimes, assisted by spark plasma conditions [8]. It is worth pointing out that no-additive pressureless sintering of Si_3N_4 has also been occasionally reported, especially, for the compound's nanopowders [9]. Powders of aluminum nitride AlN have been sintered by very much similar methods and, again, advantageous no-additive sintering conditions were noted for the nitride nanopowders [10]. One has to realize that pressureless sintering of AlN even with the help of additives requires relatively high temperatures of the order of 1700 − 1800 °C and higher whereas in a few specific cases of nanopowders lower sintering temperatures of 1400 − 1600 °C have also been successfully applied [10b, c]. As far as gallium nitride GaN is concerned, the authors of this study reported for the first time a no-additive sintering of pure [11a, b] and Mn-doped GaN nanopowders [11c] with controlled recrystallization towards mechanically robust nanoceramics. For instance, a pure GaN nanopowder was sintered under the conditions of 900 °C, 6 GPa, and 3 − 10 min. The resultant ceramics was prepared in the form of a disc of 4 mm (radius) x5 mm (height) showing an outstanding Vickers micro-hardness of 13 GPa and being composed of h-GaN with average crystallite size of *ca.* 70 − 80 nm. Higher temperatures resulted in progressing crystallite growth that could be somewhat retarded by pressure increase. The limiting factor in GaN sintering is the nitride's thermal instability above 950 − 1100 °C [12] and this poses a real challenge in sintering GaN in the composite system with AlN.

Herein, reported is a study on the *in situ* preparation of composite nanopowders of AlN and GaN, including such system admixed with a proportion of solid solution $Al_{0.5}Ga_{0.5}N$ in one of the precursor routes, and their no-additive, high-temperature and high-pressure sintering with or without recrystallization towards composite nanoceramics. The individual pure nitrides AlN and GaN are also made and processed *via* analogous routes for reference purposes. The precursor nitridation temperatures of 800 and 950 °C are used to make powders of varying average crystallite diameters in the nanosized range, with height of the latter temperature limited by thermal instability of GaN [12]. The sintering temperatures of 650 and 1000 °C are selected based upon their impact on recrystallization in this process. The temperature of 650 °C is lower than both nitride preparation temperatures and, therefore, is anticipated to be neutral to thermally induced crystal growth (sintering without recrystallization). On the other hand, the temperature of 1000 °C is higher than both those temperatures and is to contribute to crystal growth (sintering with recrystallization) – not only this, but also to reactions of available AlN and GaN towards their solid solution. By suitable modifications, initially, of the precursor chemistry and, later, of the sintering conditions a good deal of control over composition and mechanical properties of the nanoceramics is anticipated. The application of pressure is presumed to significantly accelerate sintering and, in correlation with applied temperature, put definite constraints on particle recrystallization, if desired.

2. Experimental

2.1. Preparation of precursors in the mixed bimetallic tris(dimethylamide) system $|\{Al[N(CH_3)_2]_3\}_2/\{Ga[N(CH_3)_2]_3\}_2|/NH_3$, *atomic Al:Ga = 1:1 [6b] and in individual reference systems of* $|\{Al[N(CH_3)_2]_3\}_2|/NH_3$ *[6b] and* $|\{Ga[N(CH_3)_2]_3\}_2|/NH_3$ *[6a]*

a) **Preparation of Precursor 1 *via* room temperature (RT) ineffective equilibration.** Samples of {Al[N(CH$_3$)$_2$]$_3$}$_2$, 6.36 g (20.0 mmol) and {Ga[N(CH$_3$)$_2$]$_3$}$_2$, 8.07 g (20.0 mmol) were made according to the published procedures, dissolved together in 60 mL of hexane, and stirred at RT for 10 min. This was equivalent to a negligible mixed-metal dimer formation [6b]. A few experiments were carried out with a longer stirring time of 24 h at RT. Hexane was evaporated and liquid NH_3 (60 mL) was transferred onto the solid at −78 °C. The mixture was stirred under reflux at *ca.* −33 °C for 2 h which was followed by a 2-h NH_3 boil-off at this temperature. The resulting white solid was evacuated at RT for 0.5 h affording polymeric amide-imide/imide Precursor 1.

b) **Preparation of Precursor 2 *via* reflux/effective equilibration.** Samples of {Al[N(CH$_3$)$_2$]$_3$}$_2$, 6.36 g (20.0 mmol) and {Ga[N(CH$_3$)$_2$]$_3$}$_2$, 8.07 g (20.0 mmol) were made according to the published procedures, dissolved together in 60 mL of hexane, and refluxed for 3 h. This was equivalent to *ca.* 50 % bimetallic dimer {Al/Ga[N(CH$_3$)$_2$]$_3$}$_2$, Al:Ga = 1:1, formation [6b]. The subsequent work-up was identical as above and afforded polymeric amide-imide/imide Precursor 2.

c) **Preparation of Precursors 3 and 4.** The reference amide-imide/

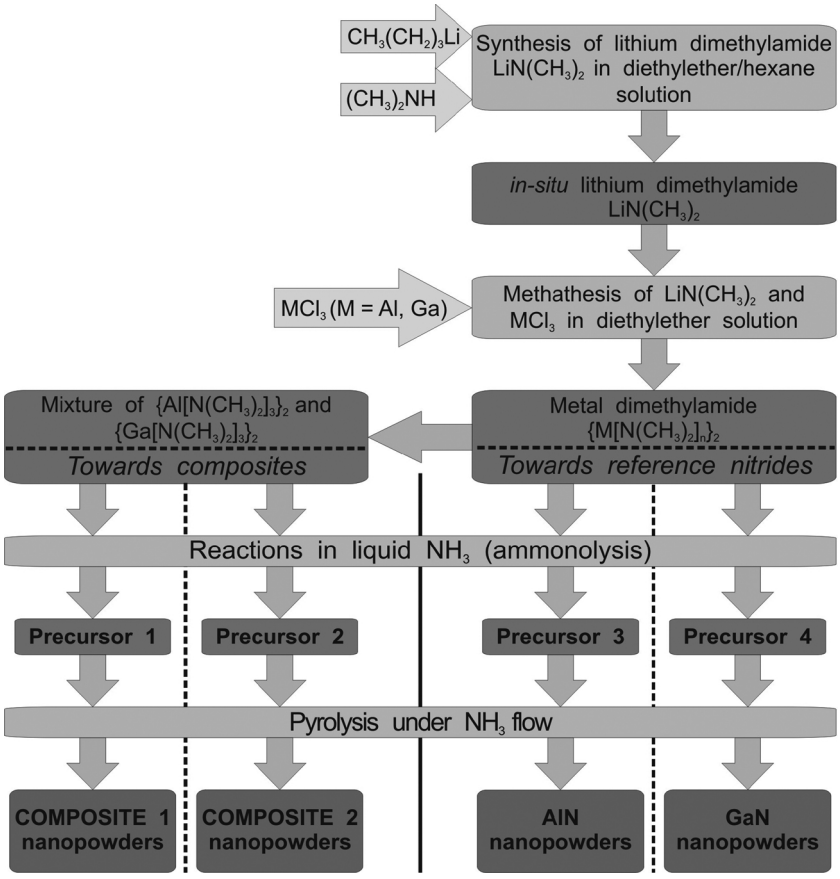

Fig. 1. Essential steps in the preparation of Al/Ga amide-imide Precursors 1-4 and their pyrolytic conversion to individual and composite metal nitride nanopowders.

imide precursors for individual nitrides AlN (Precursor 3) and GaN (Precursor 4) were made each from the respective metal tris(dimethylamide) by ammonolysis of the solid samples in liquid ammonia under the same conditions as applied for Precursors 1 and 2.

2.2. Nitridation pyrolysis

Bimetallic Al/Ga-amide-imide Precursors 1 and 2 as well as individual Al-amide-imide and Ga-imide Precursors 3 and 4, respectively, were used in pyrolysis experiments. The experiments were performed under a flow of NH_3, 0.2 L/min, 4 h at two selected temperatures, 800 and 950 °C, for each precursor loaded in an alumina boat. The products were light-colored, yellow to light grey free-flowing powders that were stored in a glove-box.

2.3. High-pressure and high-temperature sintering

The powders, that were prepared by nitridation pyrolysis, were handled in a glove-box and, at some point, sealed in glass ampoules under vacuum. Upon ampoule opening, the powders were removed and briefly handled in air prior to the high-pressure high-temperature sintering using the methodology worked out earlier by some of us [11]. Specifically, the powders were sintered for 3 min in a high pressure torroid cell at 650 and 1000 °C under the pressure of 7.7 GPa yielding dark grey to black ceramic pellets, D = 4 mm, thickness *ca.* 2 − 3 mm. For Vicker's hardness determinations on a pellet, one of its sides was polished. For other measurements, the pellets were coarsely crushed/ground in an agate mortar and used as such.

2.4. Nitride sample labeling

The powders prepared from Precursors 1 and 2 were labeled accordingly Composites 1 and 2. For example, for Precursor 1 after nitridation pyrolysis at 800 and 950 °C two products were obtained, *i.e.*, Composite 1_800 and Composite 1_950, respectively, *etc.* The powders made from Precursors 3 and 4 were individual nitrides of AlN and GaN and were similarly labeled. For example, for Precursor 3 pyrolyzed at 800 and 950 °C the two powder products were, respectively, AlN_800 and AlN_950, *etc.* The sintered ceramics had names of the related nitride powders with suitable postfixes for sintering temperature, *e.g.*, Composite 1_800_sint_650 or AlN_950_sint_1000, *etc*.

2.5. Characterization

Powder XRD determinations were done for all nitride products by Empyrean PANalytical, Cu K_α source; $2\Theta = 10 - 110^\circ$. Average crystallite sizes were evaluated from Scherrer's equation applying the Rietveld refinement method. Solid-state MAS NMR spectra were measured using the APOLLO console (Tecmag) and the 7 T/89 mm superconducting magnet (Magnex). A Bruker HP-WB high speed MAS probe equipped with the 4 mm zirconia rotor and the KEL-F cap was used to spin the sample. The ^{71}Ga MAS NMR spectra were measured at the 91.385 MHz resonance frequency spinning the sample at 10 kHz. A single 2 μs rf pulse was used, which corresponded to π/4 flip angle in the liquid. The acquisition delay used in accumulation was 4 s and 256 scans were acquired. The frequency scale in ppm was referenced to 1 M aqueous solution of $Ga(NO_3)_3$. The ^{27}Al MAS NMR spectra were measured at the 78.068 MHz resonance frequency spinning the sample at 8 kHz. A single 2 μs rf pulse was used which corresponded to π/6 flip angle in the liquid. The acquisition delay in accumulation was 1 s and 1000 scans were acquired. The frequency scale in ppm was referenced to 1 M aqueous solution of $Al(NO_3)_3$. In order to assess the magnitude of quadrupolar effects in the ^{27}Al MAS NMR spectra, a supplementary experiment was performed at 11.74 T using the Bruker Avance III

spectrometer and spinning the sample at 10 kHz. A single 0.2 us rf pulse was applied at the resonance frequency of 130.33 MHz and 6000 scans were acquired with 0.2 s repetition time. All resonance positions were uncorrected for the second-order quadrupolar shift. FT-IR determinations were carried out on Nicolet 380 spectrometer in KBr pellets made in dry-box. Standard 5-point BET specific surface areas, mesopore surface areas, and average mesopore diameter (the latter two based on BJH theory applied to the desorption part of the isotherm hysteresis) were determined by low temperature nitrogen adsorption on Micromeritics Gemini 2380. Helium densities were obtained by Micromeritics AccuPyc 1330. SEM/EDX data were acquired with a Hitachi Model S-4700 scanning electron microscope. The Vicker's hardness (H_V) tests were performed on microhardness tester FutureTech FM-700 with a 300 or 100 g-force load on a polished pellet surface, 10 s, and hardness expressed in GPa. Typically, five to ten measurements were carried out for a pellet to calculate an average H_V value and its standard deviation.

3. Results and discussion

3.1. From molecular precursors to preparation of nanopowders

The schematic diagram of the aluminum and gallium amide-imide precursor synthesis from the metals tris(dimethylamides) and precursor nitridation pyrolysis to the mixed bimetallic nitride composite or individual metal nitride nanopowders is shown in Fig. 1.

Two equilibration pathways of the starting mixed Al/Ga tris(dimethyalmide)s in hexane were employed, which were intended to result either in just a mixture of individual compounds (ineffective equilibration at RT towards Precursor 1) or in *ca.* 50 % formation of the bimetallic amide dimer admixed with the "unreacted" individual amides (effective equilibration under reflux conditions towards Precursor 2) [6b]. The latter pathway should lead to some solid solution $Al_xGa_{1-x}N$ formation upon nitridation pyrolysis of Precursor 2 at 800 and 950 °C compared to the former one and, therefore, the equilibration step should enable some control over the make-up of the resulting Composites 1 and 2. Two reference individual nitrides were prepared under the same pyrolysis conditions, *i.e.*, pure AlN from Precursor 3 and pure GaN from Precursor 4.

The FT-IR spectra (not shown) for all composites and individual reference nitrides display, when applicable, the bands at *ca.* 670 cm^{-1} for Al-N stretches in AlN and at *ca.* 570 − 580 cm^{-1} for Ga-N stretches in GaN. It is worth to note that no distinct feature(s) could be discerned in this spectral region for the plausibly overlapped specific band(s), if any, of $Al_{0.5}Ga_{0.5}N$ in the composites containing the solid solution.

The powder XRD patterns for all nitride nanopowders at two pyrolysis temperatures are included in Fig. 2. For Precursor 1-derived powders at 800 and 950 °C, virtually the same products are present yet in the bimodal particle size distributions specified by the average crystallite size D_{av}, namely, a relatively well crystallized hexagonal GaN (Composite 1_800, D_{av} = 60 nm; Composite 1_950, D_{av} = 80 nm) and much less crystallized hexagonal AlN (Composite 1_800, D_{av} = 4 nm, Composite 1_950, D_{av} = 5 nm). The set of the relatively sharp peaks corresponds to h-GaN whereas the expected similar set for h-AlN could be found upon peak deconvolution as very broad peaks located at the sharp peak bases. No indication is found for solid solution formation in both stirring times at RT, *i.e.*, 10 min and 24 h (XRD for the latter not shown) and at either of the nitridation temperatures. This was consistent with the independent nitridation of the Al-amide-imide and Ga-imide components in the ineffectively equilibrated Precursor 1, which resulted in an intimate mixture of the two nitrides in Composite 1.

A strikingly different outcome is found for Precursor 2-derived powders, *i.e.*, Composite 2_800 and Composite 2_950, of which XRD patterns can be satisfactorily deconvoluted into three hexagonal phases corresponding to h-AlN, h-GaN, and solid solution h-$Al_xGa_{1-x}N$, x = 0.4 − 0.5. Generally, a precise determination of *x* from the XRD data is hardly possible, especially, for the nanocomposites due to severe peak overlap of the phases and extreme peak broadness for the smallest nanocrystallites of AlN. In the following discussions, the composition of

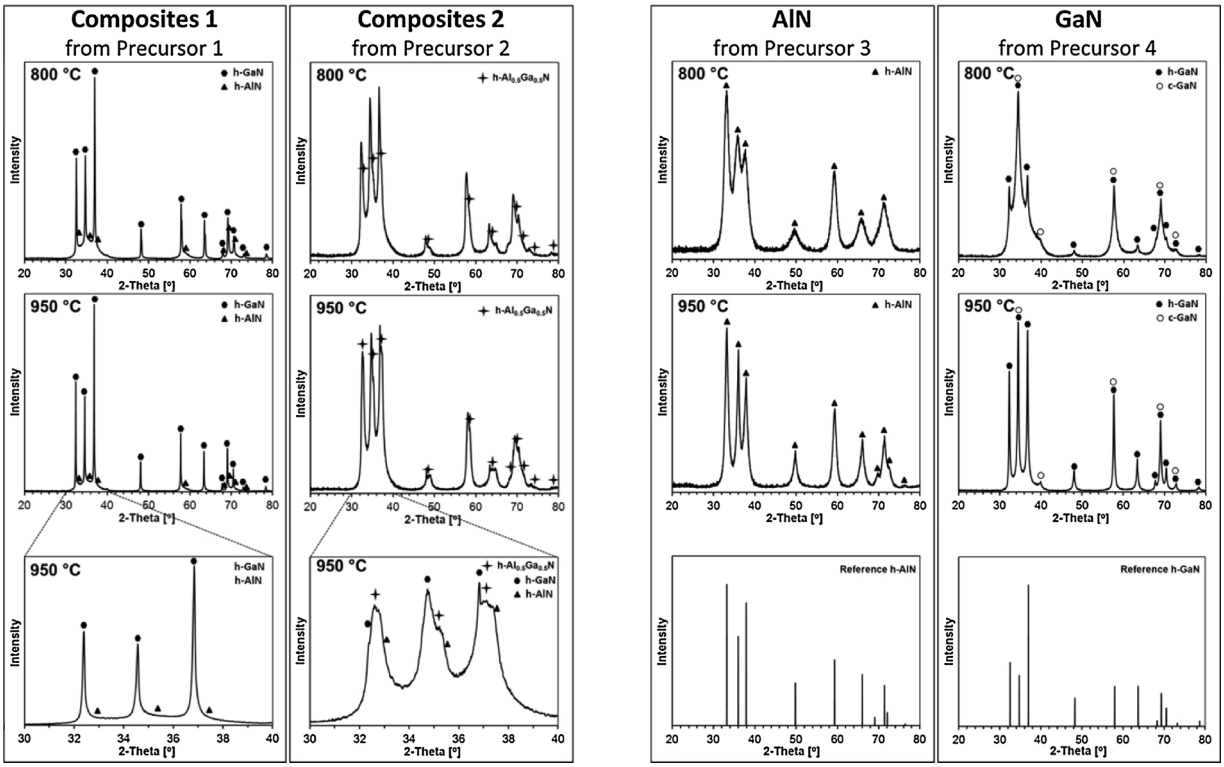

Fig. 2. Powder XRD patterns of nitride nanopowders pyrolyzed at 800 and 950 °C: left – bimetallic nitride Composites 1 and 2 with only h-$Al_{0.5}Ga_{0.5}N$ phase marked for full 20-80° range of Composite 2 and with a bottom raw showing expansions of the 30-40° range for both Composites pyrolyzed at 950 °C; right – individual nitrides AlN and GaN with a bottom raw including bar charts for hexagonal polytypes.

the solid solution will be shown for simplicity as h-$Al_{0.5}Ga_{0.5}N$. For Composite 2_800, two partially overlapped sets of the most intense peaks are assigned to h-GaN (D_{av} = 25 nm) and h-$Al_{0.5}Ga_{0.5}N$ (D_{av} = 30 nm) whereas the broad features at their bases are fitted to poorly crystallized h-AlN (D_{av} = 2 nm). Interestingly, for Composite 2_950, the same three phases are present with similar size characteristics for GaN and $Al_{0.5}Ga_{0.5}N$ (D_{av} = 27 nm) whereas AlN is relatively better crystallized, nonetheless, still in the low nanosized range (D_{av} = 4 nm).

These XRD results can be compared with data for the individual nitrides AlN and GaN prepared under the same conditions (Fig. 2, right). The average crystallite sizes D_{av}'s for h-AlN_800 and h-AlN_950 are 6 and 11 nm, respectively, which are on average twice as large as found earlier for this nitride in both composites. The pure GaN powders are, however, mixtures of the hexagonal and cubic polytypes. In particular, for GaN_800: h-GaN/c-GaN = *ca.* 1/1, D_{av} (hexagonal) = 17 nm, D_{av} (cubic) = 5 nm whereas for GaN_950: h-GaN/c-GaN = *ca.* 2/1, D_{av} (hexagonal) = 50 nm, D_{av} (cubic) = 10 nm. The higher nitridation temperature results in larger crystallites sizes and predominance of the stable hexagonal polytype, as expected. Interestingly, no c-GaN is found in the composites and the h-GaN component there shows either higher D_{av}'s in the Composite 1 powders or lower D_{av}'s in the Composite 2 powders compared with the relevant reference h-GaN sizes. It is apparent that the thinning effect in crystallite growth of the specific components in these composites is of complex nature. This is especially true for GaN with the relatively high propensity for recrystallization coupled with cubic-to-hexagonal phase conversion at these temperatures.

From the XRD study, it is clear that the equilibration stage in the preparation of the Al/Ga-tris(dimethylamide) precursors is crucial for partial formation of the RT-stable chemically mixed precursor that upon nitridation pyrolysis at 800 − 950 °C is plausibly converted to the h-$Al_xGa_{1-x}N$ component in the resulting composite h-AlN/h-GaN/h-$Al_xGa_{1-x}N$. The crystallinity of this phase after 950 °C nitridation (D_{av}, 25 − 30 nm) is of the same order as of the h-GaN component whereas the h-AlN crystallites are much smaller being in the low nanosized range (D_{av}, 2 − 4 nm). Additionally, the deconvoluted sharp components of the peaks (not shown) point out to a small share of even larger crystallites of h-GaN and/or h-$Al_xGa_{1-x}N$ in the composites whereas their (002)-peak relatively increased intensity (middle peak in the triplet of peaks at 2Θ = 30 − 40°) indicates some preferential growth *vs.* the *c* axis.

Fig. 3 shows typical in this study SEM images of the composite morphology and degree of grain uniformity as illustrated for Composite 2 nanopowders. They appear to be loose aggregates of more tightly bound much smaller agglomerates (grains), the latter of several tens to a few hundred nanometer in size. On closer inspection, those agglomerates are made of as if fused smaller particles and show some nanoporosity. In addition, quite well-faceted and relatively large hexagonal pyramid crystallites embedded in the aggregates are rarely seen, likely, for either of the h-GaN and h-$Al_xGa_{1-x}N$ well crystallized phases confirmed by XRD. It is apparent that the *in situ* made composites are naturally well homogenized down to a few tens of nanometer scale, which is also confirmed by EDX analysis for several scattered areas.

The basic characteristics of nanopowder surface properties and porosities are provided by low temperate nitrogen adsorption (total BET and mesopore BJH surface areas) and helium density measurements. For instance, the Composite 1_800 nanopowder shows the relatively high specific surface areas BET(BJH) of 73(109) m^2/g to be compared with Composite 2_800 surface areas BET(BJH) of 29(43) m^2/g both with prevailing mesoporosity. Interestingly, the values for Composite 2_950, BET(BJH) of 24(39) m^2/g, are a bit smaller but still comparable with Composite 2_800. Such an outcome is coherent with their similar crystallite size characteristics derived from XRD (see, above) and general porosity *vs.* crystallite size relationships for nanopowders [14]. It is instructive to note that the surface area of nanopowders, if prevailingly associated with nanoparticle surfaces, may reach maximum values near 300 m^2/g so the values of several tens of m^2/g are relatively high. Also, the BET(BJH) measurements reflect the surface area available for condensation of nitrogen molecules and, therefore, depend on the gas accessible porosity of tightly bound agglomerates. Helium density d_{He} is closest to the true/theoretical density and its deviation from the latter may reflect, generally, structure defects and/or closed pores unavailable to helium penetration. For AlN:GaN = 1:1 (mole basis), $d_{theor}AlN$ = 3.26 g/cm^3 and $d_{theor}GaN$ = 6.15 g/cm^3, the theoretical density of such a composite equals 4.76 g/cm^3. The determined densities for the Composites range from 4.11 g/cm^3 (Composite 1_800) to 4.24 g/cm^3 (Composite 2_950) corresponding to 86–89 % of the theoretical density, respectively. These values are similar and point out to significant closed pores occurrence in all powders.

3.2. Powder sintering towards nanoceramics

In conclusion of powder preparation, a diverse pool of individual nitrides and nitride composites was synthesized for sintering experiments. It included a range of different component nanodimensions and their particle size distributions (bimodal size distributions of AlN and GaN) and variations in the chemical make-up (binary mixtures of AlN and GaN and/or ternary mixtures of AlN, GaN, and $Al_{0.5}Ga_{0.5}N$). The high-pressure and high-temperature powder sintering was carried out at 650 and 1000 °C, 7.7 GPa, and resulted in black, mechanically hard pellets. The former temperature is lower than both powder nitridation temperatures, *i.e.*, 800 and 950 °C, preventing from temperature-induced recrystallization during sintering and, essentially, preserving the initial nanosized characteristics. The latter, on the other hand, is higher than those temperatures and expected to support both grain recrystallization and additional solid solution formation *via* reactions between available AlN and GaN to afford at the end a diverse range of nanoceramics.

It is instructive to begin discussion of the XRD data for the sintered

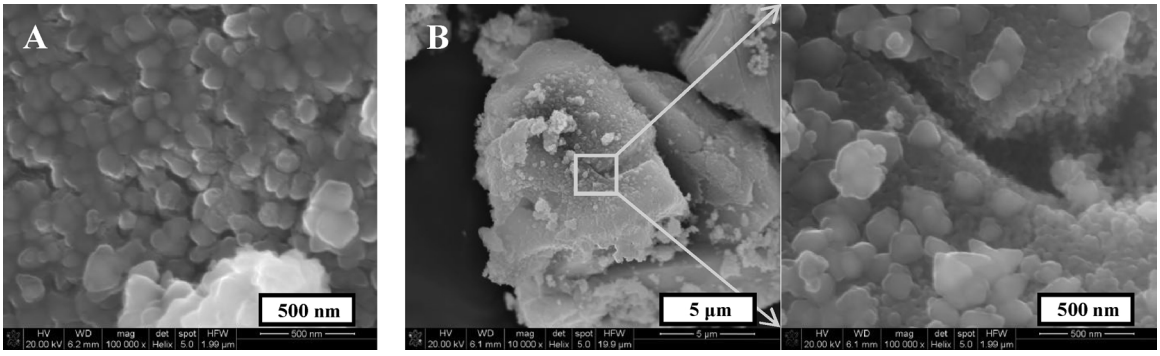

Fig. 3. Typical SEM images of nanopowders. A – Composite 2_800, B – Composite 2_950.

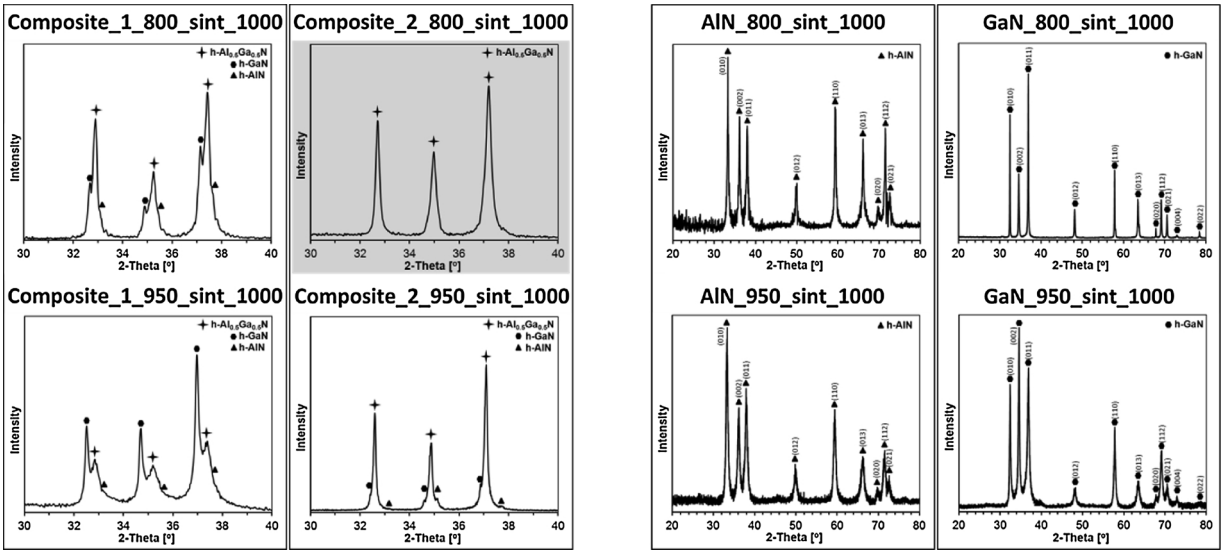

Fig. 4. Powder XRD patterns of nanoceramics prepared by sintering at 1000 °C, 7.7 GPa of various nanopowders of Composite 1 and Composite 2 – left (2Θ = 30-40°) and individual AlN and GaN – right (2Θ = 20-80°). Pattern for nanoceramics made of pure $Al_{0.5}Ga_{0.5}N$ is singled out with grey background.

pellets with Composites 1 and 2 pyrolyzed at 800 and 950 °C and then sintered at 650 °C (not shown). The pellets prepared from Composite 1 are confirmed in both cases to be mixtures of the individual nitrides, AlN and GaN. As anticipated, no solid formation takes place at this relatively low sintering temperature whereas the impact of pressure is demonstrated by markedly smaller crystallite sizes compared with those in the parent powders, *e.g.*, for Composite 1_800_sint_650 it was D_{av}(AlN) = 2 nm and D_{av}(GaN) = 13 nm to be compared with the values for the starting Composite 1_800 powder of D_{av}(AlN) = 4 nm and D_{av}(GaN) = 60 nm. This is supported by frequent observations in this study that, other things being equal, pressure cannot only restrain crystallite growth but may cause “crushing" events in the single and binary but not necessarily ternary systems. In this regard, the pressure-linked crystallite size decrease is found in all instances when the sintering temperature is in no-recrystallization regime, *i.e.*, lower than the nanopowder synthesis temperature. Also, the phenomenon appears to apply to all crystallite sizes used in this study. For the ternary systems, however, the two pellets sintered at 650 °C from both powders of Composite 2 are found to be mixtures of the same three components and in similar proportions as they are in the starting nanopowders of Composite 2_800 and Composite 2_950, namely, AlN (23–27 %, D_{av} = 10 nm), GaN (40–43 %, D_{av} = 30 nm), and $Al_{0.5}Ga_{0.5}N$ (33–34 %, D_{av} = 30 − 40 nm). This time, no clear pressure-linked crystallite size reduction is observed for any of the components. Adding to the crystallite size-related discussion of the 650 °C-sintering experiments, the D_{av}'s for pure AlN_950_sint 650 and pure GaN_950_sint_650 are 10 nm and 17 nm, respectively.

Fig. 4 shows the XRD diffraction patterns in the diagnostic range 2Θ = 30 − 40° for the nanoceramics sintered at 1000 °C from both Composite 1 and Composite 2 as well as in the extended range of 20 − 80° for the individual AlN and GaN powders all made in two ways, *i.e.*, by nitridation at 800 and 950 °C. The selected low angle 2Θ range for the wurzite-type hexagonal nitrides is characteristic of the triplet of intense peaks of which the middle one for the (002) plane is often of increased and variable relative intensity. This can be attributed to a frequently observed preferential crystal growth of the (002) plane and resulting platelet-like particle morphology.

It is interesting to note that both nanoceramics sintered at 1000 °C from Composite 1 show substantial solid solution $Al_{0.5}Ga_{0.5}N$ contents, *i.e.*, Composite 1_800_sint_1000 – 33 % with D_{av} = 75 nm and Composite 1_950_sint_1000 – 37 % with D_{av} = 24 nm. Since the starting powder composites were made of the binary mixtures of h-AlN and h-GaN, the solid solution was clearly formed during sintering by reaction of the nitrides. The remaining unreacted nitrides show a diverse crystallite size behavior upon sintering. Namely, h-AlN in Composite 1_800_sint_1000 and Composite 1_950_sint_1000 is found to increase its D_{av}'s from 4 to 64 and from 5 to 10 nm, respectively, whereas h-GaN is found either to increase its D_{av}'s from 60 to 65 nm or decrease from 80 to 64 nm, respectively. This is likely a result of both the size decreasing circumstances due to the nitride particle reactions towards solid solution and concurrent size increase *via* temperature-induced crystallite growth.

Remarkably, the nanoceramics sintered from Composite 2 are prevailingly or exclusively made of the nitrides' solid solution – Composite 2_950_sint_1000 contains 87 % whereas Composite 2_800_sint_1000 is 100 % h-$Al_{0.5}Ga_{0.5}N$, D_{av} = 49 nm. This is consistent with sintering-mediated reactions of available AlN and GaN towards their solid solution. The latter case is the first reported example of nanoceramics made of aluminum gallium nitride $Al_xGa_{1-x}N$, x = 0.5. The hexagonal lattice parameters derived from the XRD data for h-$Al_{0.5}Ga_{0.5}N$ in this materials form are for pellet 1: a = 3.175 Å, c = 5.151 Å, c/a = 1.62 and for pellet 2: a = 3.169 Å, c = 5.140 Å, c/a = 1.62. It is instructive to note that the peak intensities reflect more of the GaN intensity pattern than that of AlN and do not suggest any preferential crystal growth (compare with Fig. 2, right). These experimental cell parameters for nanoceramics can be referred to the expected values derived from Vegard's law based on theoretical calculations for AlN and GaN nanopowders to yield for the composition $Al_xGa_{1-x}N$, x = 0.5, the values of a = 3.145 Å, c = 5.075 Å, and c/a = 1.61 [5c]. It is worth to mention that other calculations predict for $Al_xGa_{1-x}N$ a positive deviation parameter for a of *ca.* 0.02 Å and a negative deviation parameter for c of *ca.* -0.04 Å [5d]. Yet, other theoretical calculations point out to distinct structure(s) for, specifically, the $Al_{0.5}Ga_{0.5}N$ composition [5e]. The input for the Vegard's law can also be the experimental cell parameters for the relevant individual nitrides sintered in this study, *i.e.*, AlN_800_sint_1000 (a = 3.12 Å, c = 4.98 Å, c/a = 1.60) and GaN_800_sint_1000 (a = 3.19 Å, c = 5.19 Å, c/a = 1.63). The Vegard's average cell parameters for $Al_{0.5}Ga_{0.5}N$ are in this case calculated as a = 3.155 Å, c = 5.085 Å, and c/a = 1.61 and compare well to the theoretically predicted ones. Both these Vegard's law-based approximations yield cell parameters that differ significantly from the ones that are determined experimentally for pure $Al_{0.5}Ga_{0.5}N$ from the current XRD data. And significantly, the parameters also do not compare favorably with the ones measured experimentally by XRD for a single crystal of the solid solution composition very close to ours, namely for $Al_{0.52}Ga_{0.48}N$ with

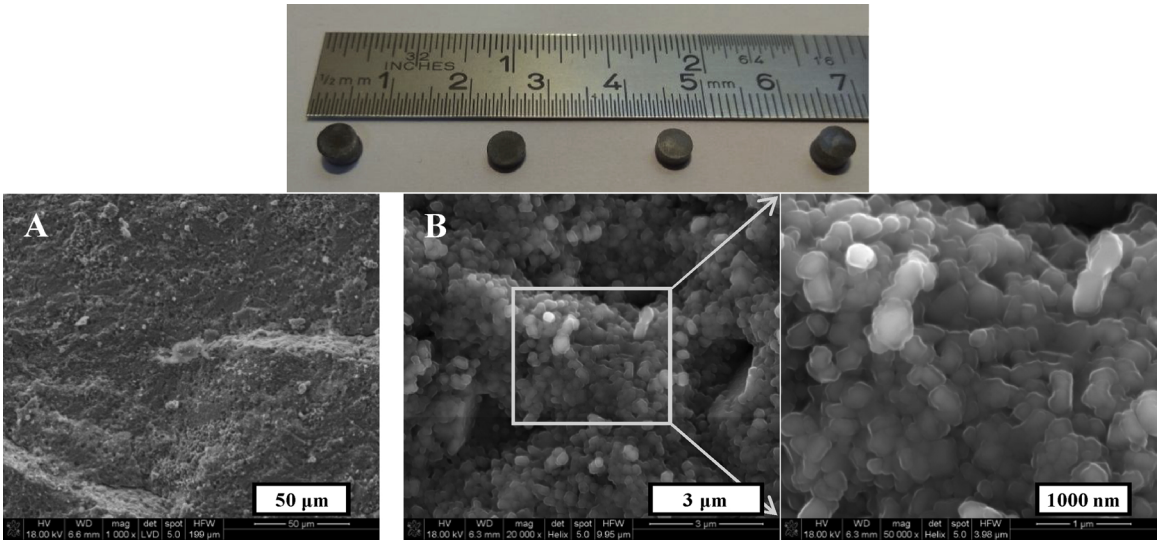

Fig. 5. Images of sintered nanoceramics. Top – snapshot of typical pellets of sintered nitride composites and individual nitrides. Bottom – SEM images of fractured nanoceramics composed exclusively of solid solution $Al_{0.5}Ga_{0.5}N$: A – low magnification of fracture, B – highest magnifications in the nanoscopic range.

a = 3.1422(4) Å and c = 5.0842(5) Å [15]. In this regard, we want to reiterate that the $Al_{0.5}Ga_{0.5}N$ nanoceramics is reactively formed under extreme high-pressure and high-temperature conditions that may have favored a specific metastable structure.

The nanoceramics prepared from pure AlN and GaN nanopowders at 650 °C are subject to the same crystallite size-related trend as observed for the composites sintered under the same conditions. Additionally, for GaN pellets there is also the absence of cubic GaN due to its conversion to the stable hexagonal polytype upon HP-HT sintering. For the AlN nanopowders, sintering at 1000 °C causes some increase of the D_{av}'s for AlN_800_sint_1000 from 6 nm to 29 nm and for AlN_950_sint_1000 from 11 nm to 20 nm. However, for the GaN nanopowders the D_{av} changes in a diverse way, namely, for h-GaN_800_sint_1000 it considerably increases from 17 nm to 160 nm whereas for h-GaN_950_sint_1000 it decreases from 50 nm to 31 nm. The latter case implies that the anticipated crystal growth of h-GaN nanocrystallites because of, merely, a slight increase in processing temperature (from 950 °C in powder preparation to 1000 °C during sintering) loses on overall to crystallite "crushing" due to the applied pressure.

The FT-IR spectra (not shown) for all composite nanoceramics contain two closely spaced sharp bands at *ca.* 670 − 680 cm^{-1} for Al-N stretches and at *ca.* 590 − 610 cm^{-1} for Ga-N stretches. The bands increased sharpness is consistent with a more definite short range ordering of the atoms upon sintering. As observed previously for the starting powders, no distinct spectral feature(s) could be found for $Al_{0.5}Ga_{0.5}N$ in the pellets.

Fig. 5 shows typical shapes of the pellets and SEM images of their fractures as exemplified by the images for nanoceramics Composite 2_800_sint_1000 composed of pure solid solution $Al_{0.5}Ga_{0.5}N$. The pictures show a uniform grainy morphology. The grain sizes are in a few hundred nanometer range and reflect a similar morphology of the parent powder of Composite 2_800 (Fig. 3A). The grains are apparently agglomerates of smaller crystallites, which are now tightly sintered inside and among themselves as seen on the highest magnification. Also, this particular nanoceramics is characteristic of a uniform net of a nearly round-shaped and seemingly closed pores with a few micrometer diameteres. This can be diserned on image A as a quite dense net of dark point areas and seen clearly on image B as regularly spaced pits. Such closed pore formation could plausibly result from massive and multidirectional mass tranfer phenomena associated with reactions of the individual nitrides AlN and GaN towards their solid solution upon sintering. Since the AlN agglomerates are composed of much more smaller and reactive crystallites compared with the GaN agglomerates, their reactive diffusion towards GaN appears to be more likely. The eventual growth of the as-formed $Al_{0.5}Ga_{0.5}N$ would, therefore, be centered around GaN agglomerates whereas the spaces initially occupied by AlN agglomerates would become the closed pores. Such circumstances are not available in HP-HT sintering under conditions that do not promote solid solution formation, *i.e.*, at 650 °C, 7.7 GPa and, accordingly, no microsized pit pores are observed in such nanoceramics.

Short range ordering properties were probed by solid state ^{27}Al and ^{71}Ga MAS NMR spectroscopy both for the powder composites and individual nitrides as well as resulting nanoceramics, and some selected spectra are shown in Fig. 6. The ^{71}Ga MAS NMR spectra for all powders are characteristic of two peaks, *i.e.*, a relatively symmetrical peak at *ca.* 325 ppm and a rather asymmetrical and broader peak at 420 − 450 ppm (Fig. 6A). This is typical for GaN nanopowders and has been a subject of an on-going discussion as to the origin of the phenomenon [12, and references therein]. We interpret the peak at 325 ppm as representing a stoichiometric hexagonal GaN whereas the broader with variable intensity, often absent band at 420 − 450 ppm as a manifestation of the Knight shift due to conduction electrons in a N-deficient areas/part of the GaN nanopowders. In a fair approximation, the presence and intensity of the latter appears to be linked to structural inhomogeneity and non-stoichiometry of GaN. In this regard, the composites from the lower pyrolysis temperature of 800 °C, namely, Composite 1_800 and Composite 2_800 show similar and relatively moderate inhomogeneity of the h-GaN component. On the other hand, the composites from 950 °C are on the extremes as confirmed by comparison of those two peaks, *i.e.*, Composite 1_950 contains markedly N-deficient h-GaN (peak at *ca.* 450 ppm more intense than peak at 325 ppm) whereas in Composite 2_950 the nitride is much better ordered compositionally (predominant 325 ppm peak). Interestingly, this is despite much better crystallinity of GaN in the former (Fig. 2) pointing out to complex interrelations among structure, composition, and electronic properties of GaN nanopowders. In striking contrast with the appearance of the ^{71}Ga MAS NMR resonances, the ^{27}Al MAS NMR spectra for the composites are very simple and similar to each other (Fig. 6A). They all contain one asymmetrical band centered at 114 − 115 ppm as reported for quadrupolar ^{27}Al nuclei in hexagonal AlN [13]. There is no indication for significantly different resonance conditions of the nuclei if present in the solid solution $Al_{0.5}Ga_{0.5}N$ to the extent of a distinct peak evolution or significant peak shift. This is confirmed by the typical/singular appearance of the ^{27}Al resonances in Composite 2 powders from both nitridation temperatures, which contain $Al_xGa_{1-x}N$. The ^{71}Ga MAS NMR

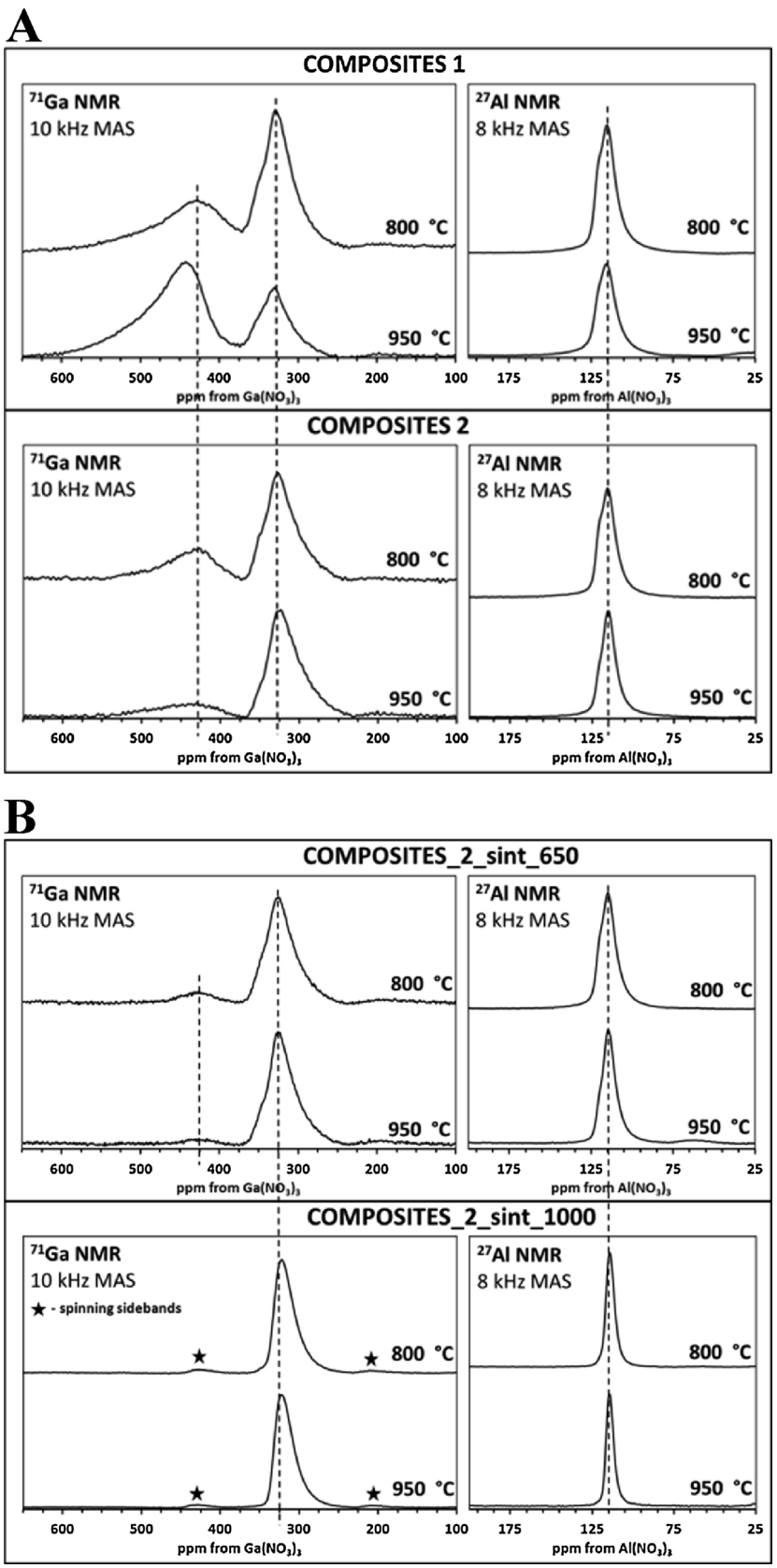

Fig. 6. Solid-state ^{27}Al and ^{71}Ga MAS NMR spectroscopy for selected composite powders and nanoceramics: A – powder Composites 1 and 2 each pyrolyzed at 800 and 950 °C, B – nanoceramics prepared from Composite 2 at 650 and 1000 °C. Dashed lines are eye-guides for typical peak positions.

spectra for the sintered Composite 2 powders, shown to have significant quantities of $Al_{0.5}Ga_{0.5}N$ (*e.g.*, 100 % in Composite 2_800_sint_1000), are characteristic of the prevailing or exclusive lower field resonance now at 323 − 324 ppm, *i.e.*, 1 − 2 ppm at higher fields compared with the parent composite powders (Fig. 6B). The Knight shift peak at *ca.* 450 ppm is, generally, of profoundly decreased intensity and not present at all in nanoceramics made of the pure solid solution. The ^{27}Al NMR spectra for the nanoceramics appear to have unaltered chemical shifts while becoming sharper and more symmetrical compared with the composite powders (Fig. 6B). In summary of this aspect, the NMR spectroscopy confirms the presence of the phases elaborated by XRD and provides with valuable data on their diverse close range and electronic properties. In particular, the first reported ^{71}Ga and ^{27}Al MAS NMR spectra support the highly ordered, stoichiometrically and electronically well-defined structure of pure $Al_{0.5}Ga_{0.5}N$ nanoceramics.

Regarding helium density measurements, as a reminder, the theoretical density for AlN:GaN = 1:1 (mole basis) composites equals 4.76 g/cm^3. The determined densities for the nanoceramics are in the range 4.25–4.50 g/cm^3 for various samples of Composite 1-sintered pellets (corresponding to 89–95 % of theoretical) and 4.00–4.24 g/cm^3 for Composite 2-sintered pellets (corresponding to 84–89 % of theoretical). When compared with the starting powder densities, this indicates overall some increase of the composites densities upon sintering but, also, points out to some residual closed pore porosity there. Interestingly, very much similar trends are noted for sintering of the individual powders of AlN and GaN. For AlN, the starting powders densities are in the theoretical 88–89 % range to be compared with the 88–92 % range for the resulting AlN nanoceramics. And for GaN, the powder densities in the theoretical range 84–86 % are compared with the 85–92 % range for the GaN nanoceramics. For both pure nitride and all composite powders, consistent helium density increases are noted upon sintering while never exceeding 95 % of the theoretical value. The persistence of closed pore porosity is likely associated with extensive mass transfer upon HP-HT sintering, especially, in the composite systems with the-then reactive nitride solid solution formation. In this regard, the density for the pellet made of pure $Al_{0.5}Ga_{0.5}N$ is 4.00 g/cm^3, 84 % of theoretical, being the lowest among pellets. It is very conceivable that the application of longer sintering times could favor more efficient diffusion and mass transfer phenomena to significantly eliminate such closed porosity.

The results of the Vicker's hardness test for the nanoceramics are shown in Table 1. The values of Hv's are to be compared with the reported Hv's for monocrystalline AlN and GaN, *ca.* 18 and 11 GPa at RT [16a], respectively. They can also be referenced to first-principles theoretical calculations of Hv for "AlGaN" under increased pressures, which for ambient to low pressures predict Hv of *ca.* 20 GPa [16b].

Both pure nitride nanoceramics show Hv's exceeding 10 GPa with the maximum values for AlN_800_sint_650 and GaN_950_sint_1000 of 16.1 GPa and 17.4 GPa, respectively. It is interesting to note that the Hv values for the GaN ceramics are in most cases larger than the reference value of 11 GPa whereas those for AlN ceramics are somewhat smaller than the reference value of 18 GPa. In the case of GaN, the applied powder preparation and sintering temperatures are close to the stability range of the nitride of *ca.* 950 − 1100 °C [12a, b] and both are interrelated in positively effecting diffusion rates during sintering to yield firmly, and homogeneously structured ceramics. In this case, the applied pressure has also a diverse effect on the nitride's average crystallite size as discussed earlier in the XRD data section. For AlN, the powder preparation and sintering conditions are rather mild and not limited by stability issues, and do not promote substantial mass transport/recrystallization rates as evident from rather moderate crystallite size changes from the XRD determinations. The interplay of both applied temperatures (preparation and sintering) and sintering pressure apparently creates conditions for not as efficient diffusion/recrystallization as previously and results in, relatively, more weakly structured ceramics. It is important to realize, however, that the Hv's for the AlN nanoceramic are still advantageously high. Also, the spread of the Hv's for both pure nitride nanoceramics clearly points out to realistic possibilities of controlling the hardness by suitable modifications of the powder preparation and sintering conditions.

In general, the Hv hardness of the sintered composites is relatively high but on average a bit lower compared to both sintered pure nitrides. Several of the composite nanoceramics show Hv's in the range of being equal or higher than the literature reference value of 11 GPa for single crystalline GaN whereas being short of reaching the level of 18 GPa for single crystalline AlN, not to mention the theoretical value of *ca.* 20 GPa [16b]. In this regard, the highest Hv of 15.2 GPa is noted for Composite1_950_sint_1000 with a rather moderate amount of the nanosized solid solution $Al_{0.5}Ga_{0.5}N$, *i.e.*, 37 %, D_{av} = 24 nm, reactively formed during sintering. It is instructive to note that, here, the temperature spread between powder preparation and sintering is merely 50 °C and the driving force for solid solution formation during sintering is, therefore, rather small. If one compares this material with Composite 1_800_sint_1000 showing Hv of 9.5 GPa while having a similar proportion of $Al_{0.5}Ga_{0.5}N$, 33 %, the clearly lower hardness could be linked to higher recrystallization rates of the solid solution having now D_{av} = 75 nm, likely, due to much larger aforementioned temperature spread of 200 °C. It is obvious that both the proportion of the solid solution and

Table 1
Vicker's hardness test results Hv for composite and individual nitride nanoceramics. (i) In cases shown with asterisk*, cracks extending to corners are observed, especially, for the typical 300 g load so reliable determinations could be done only with the 100 g load. (ii) Hv for pure $Al_{0.5}Ga_{0.5}N$ nanoceramics is singled out with grey background.

COMPOSITE NITRIDE NANOCERAMICS		INDIVIDUAL NITRIDE NANOCERAMICS	
Sample	H_V (*SD*) [GPa] *(100 g load)	Sample	H_V (*SD*) [GPa] *(100 g load)
Composite 1_800_sint_650: pellet 1 pellet 2	 11.9 (*0.5*) 12.9 (*1.0*)	GaN_800_sint_650: pellet 1 pellet 2	 13.6 (*0.5*) 15.0 (*0.9*)
Composite 1_800_sint_1000	9.5 (*1.6*)	GaN_800_sint_1000	10.0 (*0.8*)
Composite 1_950_sint_650	11.7 (*0.9*)	GaN_950_sint_650	10.6 (*0.6*)
Composite 1_950_sint_1000	15.2 (*0.6*)	GaN_950_sint_1000	17.4 (*0.9*)
Composite 2_800_sint_650	13.0 (*1.1*)	AlN_800_sint_650	16.1 (*0.7*)*
Composite 2_800_sint_1000	3.8 (*0.8*)*	AlN_800_sint_1000	12.3 (*0.9*)*
Composite 2_950_sint_650	11.9 (*1.0*)	AlN_950_sint_650	14.7 (*0.7*)
Composite 2_950_sint_1000	7.7 (*1.5*)	AlN_950_sint_1000	14.7 (*0.7*)

its average crystallite size are important factors in hardness development. This is further confirmed by the distinctly low Hv of 3.8 GPa for the nanoceramics made exclusively of $Al_{0.5}Ga_{0.5}N$ (Composite 2_800_sint_1000) and a rather low Hv of 7.7 GPa for the nanoceramics made mostly (87 %) of $Al_{0.5}Ga_{0.5}N$ (Composite 2_950_sint_1000). We think that the important clues as to the main causes of this behavior lie in the low helium densities and specific SEM morphology features discussed earlier. The reactive formation of $Al_{0.5}Ga_{0.5}N$ from the nitrides and associated crystal growth phenomena cause the formation of relatively large closed pit pores under the sintering conditions. A resulting net of such pores is quite uniformly spread over pellet's volume and has a detrimental impact on its hardness. Further studies will address this issue, specifically, for the novel $Al_{0.5}Ga_{0.5}N$ nanoceramics by optimizing both the powder preparation (towards maximizing $Al_{0.5}Ga_{0.5}N$ contents) and powder sintering (increased sintering times) stages.

4. Conclusions

The application of the metal tris(dimethylamide)/ammonolysis precursor chemistry enabled the preparation of a diverse pool of solid precursors to nanopowders of both individual AlN and GaN nitrides and their various *in-situ* synthesized composites including those containing some solid solution $Al_{0.5}Ga_{0.5}N$. The nanopowders were subjected to no-additive, high-pressure and high-temperature sintering at 650 and 1000 °C, 7.7 GPa, 3 min, to afford mechanically compact nanoceramics. A range of characterization methods helped in getting an in-depth insight into the chemical and structural changes both in the powder preparation stage and during sintering. The individual nitrides yielded nanoceramics showing high Hv hardness nearing or exceeding the reference values for the relevant monocrystalline samples. The composite nanoceramics had also high Hv values whereas some of them were detrimentally effected by the presence of $Al_{0.5}Ga_{0.5}N$ formed during sintering *via* concurrent evolution of a net of microsized closed pores.

Declaration of Competing Interest

The authors declare that they have no known competing financial interests or personal relationships that could have appeared to influence the work reported in this paper.

Acknowledgement

The study was funded by Polish NCN Grant No. 2017/25/B/ST5/01032.

References

[1] S. Podsiadło, Nitrides, PWN, 2014 ISBN: 978-83-01-17898-7.
[2] S. Nakamura, Background story of the invention of efficient InGaN blue-light-emitting diodes (Nobel lecture), Angew. Chem. Int. Ed. 54 (2015) 7770–7788.
[3] (a) M. Drygas, P. Jelen, M. Radecka, J.F. Janik, Ammonolysis of polycrystalline and amorphized gallium arsenide GaAs to polytype-specific nanopowders of gallium nitride GaN, RSC Adv. 6 (2016) 41074–41086 and references therein;
(b) J.A. Jegier, S. McKernan, A.P. Purdy, W.L. Gladfelter, Chem. Mater. 12 (2000) 1003–1010.
[4] A. Iwata, J. Akedo, Hexagonal to cubic crystal structure transformation during aerosol deposition of aluminum nitride, J. Cryst. Growth 275 (2005) e1269–e1273.
[5] (a) R. Garcia, S. Srinivasan, O.E. Contreras, A.C. Thomas, F.A. Ponce, $Al_xGa_{1-x}N$ ($0<x<1$) nanocrystalline powder by pyrolysis route, J. Cryst. Growth 308 (2007) 198–203;
(b) E. Lopez-Apreza, J. Arriaga, D. Olguin, *Ab initio* calculation of structural and electronic properties of $Al_xGa_{1-x}N$ and $In_xGa_{1-x}N$ alloys, Rev. Mex. Fis. 56 (2010) 183–194;
(c) A.M. Herrera, R. Garcia, G. Garcia, Erick Gastellou, F. Nieto, G.A. Hirata, O.E. Contreras, C. Morales, E. Rosendo, T. Diaz, Experimental determination of the pyrolysis temperatures of an organometallic complex to obtain $Al_xGa_{1-x}N$ powders, J. Alloys Compd. 775 (2019) 109–115;
(d) B.T. Liou, S.H. Yen, Y.K. Kuo, Vegard's law deviation in band gaps and bowing parameters of the wurtzite III-nitride ternary alloys, Proc. SPIE 5628, Semiconductor Lasers and Applications II, 20 January (2005);
(e) L.C. Xu, R.Z. Wang, H. Yan, Order structures of $Al_xGa_{1-x}N$ alloys: first-principles predictions, J. Phys. Chem. C 116 (2012) 1282–1285.
[6] (a) J.F. Janik, R.L. Wells, Gallium imide, $\{Ga(NH)_{3/2}\}_n$, a new polymeric precursor for gallium nitride powders, Chem. Mater. 8 (1996) 2708–2711;
(b) J.F. Janik, R.L. Wells, J.L. Coffer, J.V.St. John, W.T. Pennington, G.L. Schimek, Nanocrystalline aluminum nitride and aluminum/gallium nitride nanocomposites *via* transamination of $[M(NMe_2)_3]_2$, M = Al, Al/Ga(1/1), Chem. Mater. 10 (1998) 1613–1622;
(c) J.L. Coffer, T. Waldek Zerda, R. Appel, R.L. Wells, J.F. Janik, Micro-Raman investigation of nanocrystalline GaN, AlN, and an AlGaN composite prepared from pyrolysis of metal amide-imide precursors, Chem. Mater. 11 (1999) 20–22.
[7] (a) D. Rafaja, C. Wustefeld, M. Motylenko, C. Schimpf, T. Barsukova, M.R. Schwarzb, E. Kroke, Interface phenomena in (super)hard nitride nanocomposites: from coatings to bulk material, Chem. Soc. Rev. 41 (2012) 5081–5101;
(b) Z.Z. Fang, H. Wang, Densification and grain growth during sintering of nanosized particles, Int. Mater. Rev 53 (2008) 326–352;
(c) K. Lu, Sintering of nanoceramics, Int. Mater. Rev. 53 (2008) 2–38.
[8] (a) Y.S. Duan, N. Liu, J.X. Zhang, H. Zhang, X.G. Li, Cost effective preparation of Si_3N_4 ceramics with improved thermal conductivity and mechanical properties, J. Eur. Ceram. Soc. 40 (2020) 298–304;
(b) Q. Zhi, B. Wang, S. Zhao, Z. Zhang, Y.C. Deng, N.L. Zhang, J.F. Yang, Synthesis and mechanical properties of highly porous ultrafine-grain Si3N4 ceramics via carbothermal reduction-nitridation combined with liquid phase sintering, Ceram. Int. 45 (2020) 21359–21364;
(c) J.J. Yu, W.M. Guo, W.X. Wei, H.T. Lin, C.Y. Wang, Fabrication and wear behaviors of graded Si_3N_4 ceramics by the combination of two-step sintering and beta-Si_3N_4 seeds, J. Eur. Ceram. Soc. 38 (2018) 3457–3462;
(d) L.L. Yang, A. Ditta, B. Feng, Y. Zhang, Z. Xie, Study of the comparative effect of sintering methods and sintering additives on the microstructure and performance of Si_3N_4 ceramic, Materials 12 (2019) 2142.
[9] (a) Z. Krstic, V.D. Krstic, Silicon nitride: the engineering material of the future, J. Mater. Sci. 47 (2012) 535–552;
(b) B.S. Bal, M.N. Rahaman, Orthopedic applications of silicon nitride ceramics, Acta Biomater. 8 (2012) 2889–2898;
(c) F.F. Lange, The sophistication of ceramic science through silicon nitride studies, J. Ceram. Soc. Jpn. 114 (2006) 873–879.
[10] (a) H. Jiang, X.H. Wang, G.F. Fan, W. Lei, M. Fu, X.C. Wang, F. Liang, W.T. Lu, Effect of hot-pressing sintering on thermal and electrical properties of AlN ceramics with impedance spectroscopy and dielectric relaxations analysis, J. Eur. Ceram. Soc. 39 (2019) 5174–5180;
(b) Y.L. He, H.M. Wu, Investigation on low-temperature sintered AlN nanoceramics with high thermal conductivity, Int. J. Appl. Ceram. Technol. 16 (SI) (2019) 2101–2106;
(c) Q. He, M.L. Qin, M. Huang, H.Y. Wu, H.F. Lu, H. Wang, X.D. Mu, Y.L. Wang, X.H. Qu, Synthesis of highly sinterable AlN nanopowders through sol-gel route by reduction-nitridation in ammonia, Ceram. Int. 45 (2019) 14568–14575;
(d) H.M. Lee, K. Bharathi, D.K. Kim, Processing and characterization of aluminum nitride ceramics for high thermal conductivity, Adv. Eng. Mater. 16 (2014) 655–669;
(e) L.M. Sheppard, Aluminum nitride – a versatile but challenging material, Am. Ceram. Soc. Bull. 69 (1990) 1801–1812.
[11] (a) J. Borysiuk, P. Caban, W. Strupinski, S. Gierlotka, S. Stelmakh, J.F. Janik, TEM investigations of GaN layers grown on silicon and sintered GaN nano-ceramic substrates, Cryst. Res. Tech. 42 (2007) 1291–1296;
(b) J.F. Janik, M. Drygas, C. Czosnek, B. Pałosz, S. Gierlotka, S. Stelmakh, E. Grzanka, G. Kalisz, A. Swiderska-Sroda, M. Leszczynski, G. Nowak, R. Czernecki, Polish Patent No. 378458, 29.02.2012, WUP 02/12 (in Polish).
(c) M. Drygas, J.F. Janik, J. Gosk, S. Gierlotka, B. Palosz, A. Twardowski, Structural and magnetic properties of ceramics prepared by high-pressure high-temperature sintering of manganese-doped gallium nitride nanopowders, J. Eur. Ceram. Soc. 36 (2016) 1033–1044
[12] (a) M. Drygas, Z. Olejniczak, E. Grzanka, M.M. Bucko, R.T. Paine, J.F. Janik, Probing the structural/electronic diversity and thermal stability of various nanocrystalline powders of gallium nitride GaN, Chem. Mater. 20 (2008) 6816–6828;
(b) M. Drygas, M.M. Bucko, Z. Olejniczak, I. Grzegory, J.F. Janik, High temperature chemical and physical changes of the HVPE-prepared GaN semiconductor, Mater. Chem. Phys. 122 (2010) 537–543;
(c) M. Tansho, T. Suehiro, T. Shimizu, Constancy of the quadrupolar interaction product in nanocrystalline gallium nitride revealed by ^{71}Ga MAS NMR shift distribution, Solid State Nucl. Mag. Res. 97 (2019) 25–30.
[13] W.S. Jung, S.K. Ahn, Monitoring the conversion of α-alumina to AlN under a flow of nitrogen by Al-27 MAS NMR spectroscopy, J. Mater. Sci. Lett. 16 (1997) 1573–1575.
[14] M. Drygas, J.F. Janik, Modeling porosity of high surface area nanopowders of the gallium nitride GaN semiconductor, Mater. Chem. Phys. 133 (2012) 932–940.
[15] A. Belousov, S. Katrych, K. Hametner, D. Gunther, J. Karpinski, B. Batlogg, $Al_xGa_{1-x}N$ bulk crystal growth: crystallographic properties and p–T phase diagram, J. Cryst. Growth 312 (2010) 2585–2592.
[16] (a) I. Ionenaga, Mechanical stability of power device materials high temperature hardness of SiC, AlN and GaN, Chem. Sus. Dev. 9 (2001) 19–21;
(b) N. Kishore, V. Nagarajan, R. Chandiramouli, Mechanical and electronic properties under high pressure on AlGaN and InGaN compounds – a first-principles perspective, Mater. Res. Express 6 (2019) 015052.